Large Anisotropy of Electrical Properties in Layer-Structured In$_2$Se$_3$ Nanowires

Hailin Peng, Chong Xie, David T. Schoen, and Yi Cui*

Department of Materials Science and Engineering, Stanford University, Stanford, California 94305

ABSTRACT

Layer-structured indium selenide (In$_2$Se$_3$) nanowires (NWs) have large anisotropy in both shape and bonding. In$_2$Se$_3$ NWs show two types of growth directions: [11−20] along the layers and [0001] perpendicular to the layers. We have developed a powerful technique combining high-resolution transmission electron microscopy (HRTEM) investigation with single NW electrical transport measurement, which allows us to correlate directly the electrical properties and structure of the same individual NWs. The NW devices were made directly on a 50 nm thick SiN$_x$ membrane TEM window for electrical measurements and HRTEM study. NWs with the [11−20] growth direction exhibit metallic behavior while the NWs grown along the [0001] direction show n-type semiconductive behavior. Excitingly, the conductivity anisotropy reaches 10^3–10^6 at room temperature, which is 1−3 orders magnitude higher than the bulk ratio.

Nanowires (NWs) are anisotropic in shape and have been explored in many applications including nanoelectronics,[1,2] nanophotonics,[3,4] biosensors,[5] thermoelectrics,[6,7] and energy conversion.[8–12] The properties of NWs depend not only on their shape anisotropy but also on their crystallographic anisotropy.[13] The vapor−liquid−solid (VLS) growth mechanism has been demonstrated to have control over NW size, position, and orientation.[13–15] Layer-structured In$_2$Se$_3$ has received considerable attention in our group and others because of the large bonding anisotropy of their layered crystal structure and their potential applications in solar cells,[16] batteries,[17] and phase change memory devices.[18,19] The NW morphology can afford an efficient charge carrier transport pathway while maintaining a large surface-to-volume ratio, and small scale cross section for these applications.[8–10,20]

Previously, it was found that In$_2$Se$_3$ NWs grown by the Au-catalyzed VLS method have two distinct growth directions: [11−20] along the layer and [0001] perpendicular to the layer.[21,22] The bonding is strongly covalent within the layer but has a weak van der Waals nature between the layers.[23] Structural or compositional anisotropy normally implies a large anisotropy in electronic band structure. Direct correlation of electrical properties with structure in NWs with different crystallographic growth directions is important. Herein, we have developed a powerful technique combining high-resolution transmission electron microscopy (TEM) and individual NW electrical transport measurement, which allows us to correlate directly the electrical properties and structure of the same NWs. The electrical conductivity, gate response, and temperature dependence are very different for NWs with different growth directions. In$_2$Se$_3$ NWs along the [11−20] growth direction typically have a superlattice structure and exhibit metallic behavior with the conductivities of 100−500 S/cm, while the NWs along the [0001] direction show n-type semiconductive behavior with the conductivities of 0.0005−0.025 S/cm. The conductivity anisotropy between these two growth directions is in the range of 10^3–10^6.

Figure 1A shows the hexagonal structure of α phase In$_2$Se$_3$, which has tetrahedral covalent bonding between In and Se within layers of Se−In−Se−In−Se.[23] The surface of each layer is terminated with Se atoms so that the layers are linked together only by weak van der Waals interactions. The space group is $P6_3$ with hexagonal lattice constants $a = b = 0.4016$ nm and $c = 1.9222$ nm. Layer stacking is along the c direction. Bulk In$_2$Se$_3$ usually exists in the form of quasi-two-dimensional flakes or platelets owing to this anisotropic bonding. Our single-crystalline In$_2$Se$_3$ NWs were prepared via the VLS mechanism in a Au catalyst-assisted vapor transport method reported previously.[21] The dominant growth direction for In$_2$Se$_3$ NWs is along [11−20], which is parallel to the layer or perpendicular to the c axis (Figure 1B). With 20 nm diameter Au nanoparticles as catalysts, the [11−20] NWs have a nanoribbon morphology with widths of 50−300 nm and heights of 20−40 nm. The height reflects roughly the diameter of the catalysts although the width is

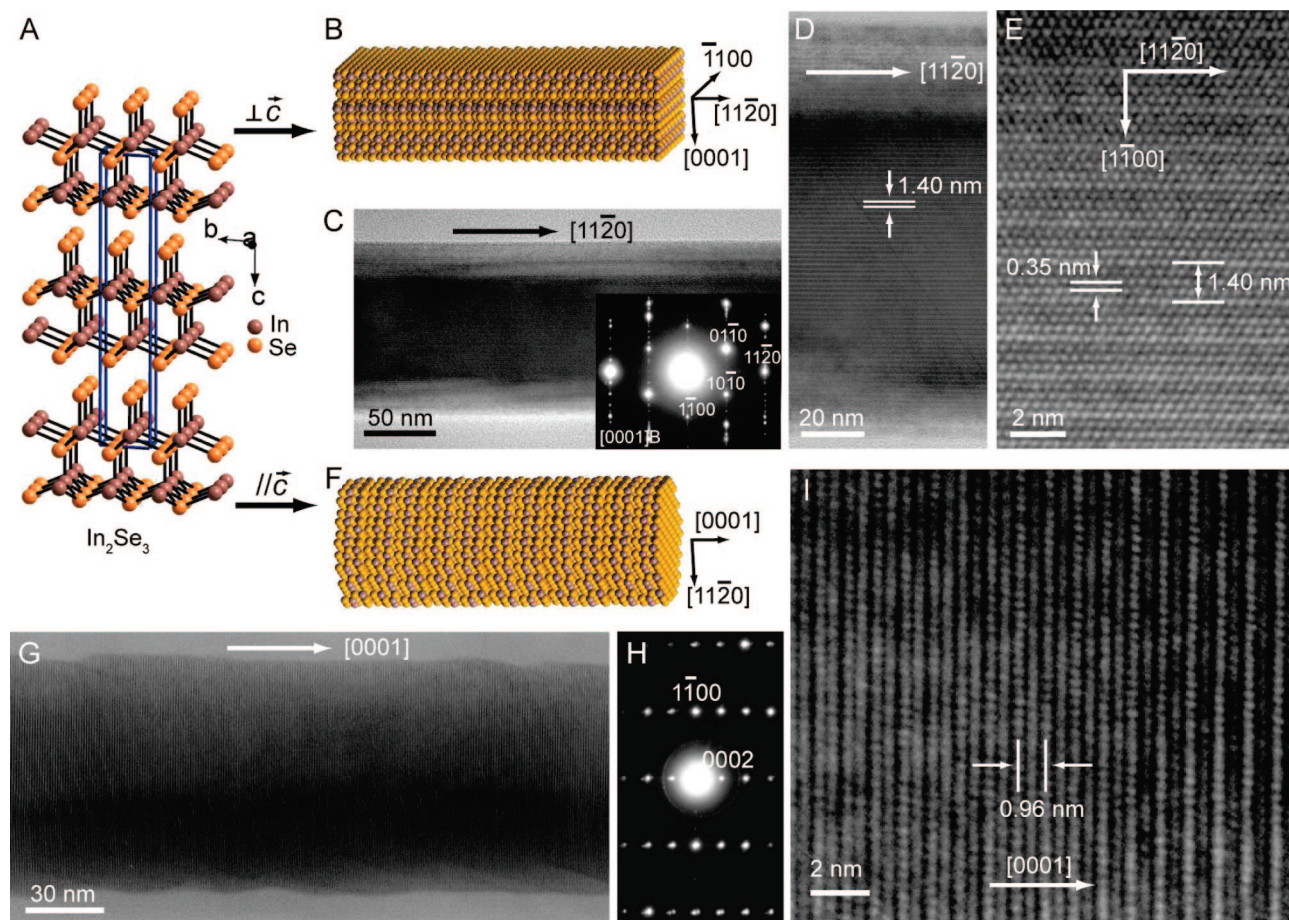* To whom correspondence should be addressed. E-mail: yicui@stanford.edu.

Figure 1. (A) Layered crystal structure of bulk In$_2$Se$_3$ based on the tetrahedral bonding of the Se−In−Se−In−Se layers. (B) Space-filling structural model for the layered In$_2$Se$_3$ NW with the [11−20] growth direction. (C) Low-magnification TEM image of a single-crystalline hexagonal In$_2$Se$_3$ NW with the [11−20] growth direction. Inset: corresponding SEAD pattern. (D,E) High-magnification TEM image of the NW with superlattice structure perpendicular to the [11−20] growth direction. (F) Space-filling structural model for the layered In$_2$Se$_3$ NW with the [0001] growth direction. (G) TEM image of a layered In$_2$Se$_3$ NW with the [0001] growth direction. (H) Corresponding SAED pattern. (I) HRTEM image of the In$_2$Se$_3$ NW with the [0001] growth direction.

much larger. We think that this is due to the highly anisotropic bonding of In$_2$Se$_3$. Right after the NW nucleation, the width and height are expected to be similar, which are defined by the VLS catalyst size. During the NW growth, the anisotropic bonding plays an important role on the growth kinetics of different crystal surfaces. The top and bottom surfaces of the [11−20] NWs are terminated with Se atoms, which are low energy surfaces which resulted from the weak van der Waals force, so that addition of atoms are not favored. The two edge surfaces of nanoribbons, however, have a large number of dangling covalent bonds, which add atoms directly from the gas phase or via diffusion from the top or bottom surfaces. Equivalently, vapor−solid (VS)[24] overgrowth also occurs at the edge surfaces of the layer-structured NWs[25] in addition to the VLS growth. The selected-area electron diffraction (SAED) pattern taken along the [0001] zone axis shows a hexagonal spot pattern, confirming the single-crystalline hexagonal phase with [11−20] growth direction (Figure 1C inset). Extra spots can be found in the diffraction pattern along the NW width direction, which has four times of the (1−100) plane distance. High-resolution TEM (HRTEM) images recorded from a segment of the NW exhibits the ordering feature across its

entire width with uniform periodicity of 1.40 nm (Figure 1D,E). Each period consists of four (1−100) planes. This superlattice structure is suggested to be caused by vacancy ordering[26] inside the In$_2$Se$_3$ NW during growth. Similar phenomenon were also found in previous reports on In$_2$Se$_3$ thin film[27,28] and other materials.[29–31] HRTEM study also shows that the NWs have smooth surfaces with very little (<1 nm) amorphous coating. The different contrast in TEM images (Figure 1C) is due to the thickness contrast in the regions near the edges of the NW.

In addition to the dominating [11−20] growth direction, a fraction of In$_2$Se$_3$ NWs have the [0001] growth direction, perpendicular to the layers. As shown in Figure 1F, the In$_2$Se$_3$ NW structure can be viewed as stacked layers packing along the [0001] direction via a weak van der Waals interaction. The [0001] NWs also have very little surface oxide although their side surfaces are rough (Figure 1G), in contrast to the smooth surfaces of the [11−20] NWs. This is presumably due to the weak bonding nature between layers. The periodicity of alternating bright and dark fringes along the growth direction is ∼0.96 nm, corresponding to the (0002) planes of hexagonal In$_2$Se$_3$. The SAED pattern (Figure 1H)
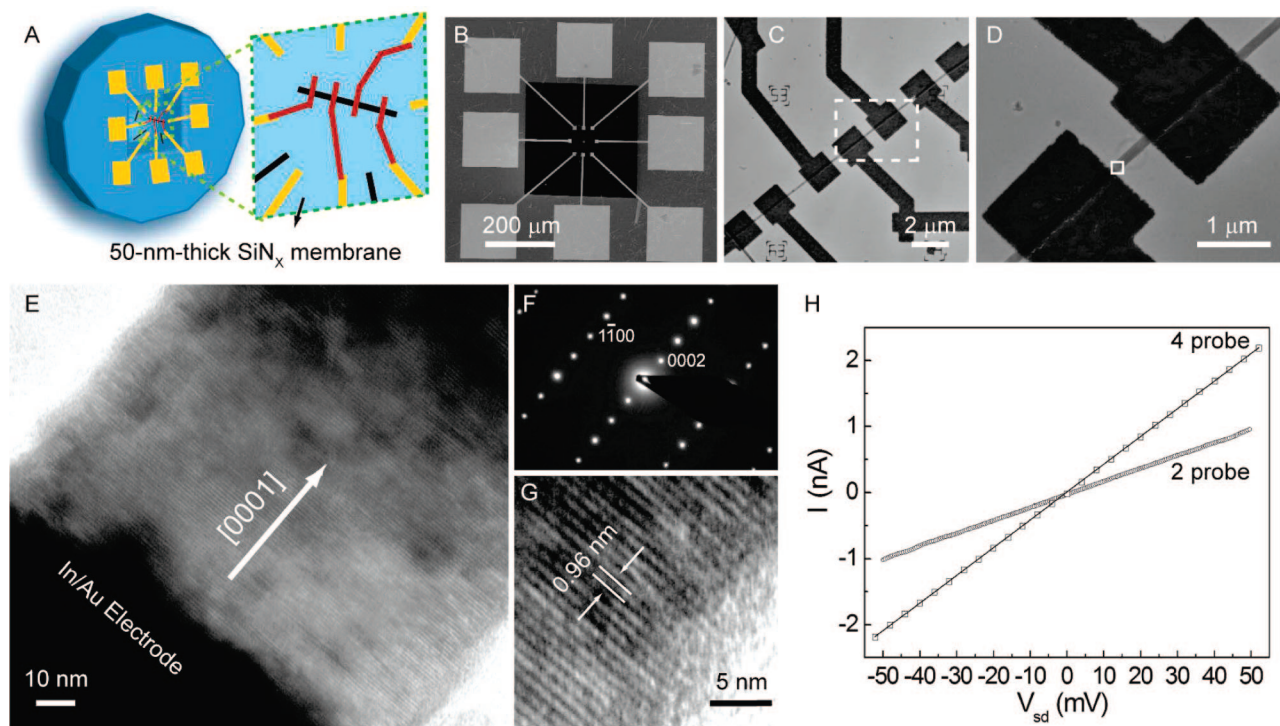
Figure 2. (A) Schematic illustration of individual NW device fabricated on 50 nm thick SiN_x membrane TEM grid with NWs in black, In/Au contact in red, and other metal electrodes in yellow. (B) Low-magnification SEM image of a representative NW TEM device. (C) TEM image of an individual NW contacted with the In/Au electrodes on TEM grid. (D) A magnified TEM image taken from the rectangular area in C. (E) High-magnification TEM image of NW contacted with the electrode taken from the rectangular area in D, showing the [0001] growth direction. (F) SAED pattern of the NW. (G) HRTEM image of the NW with the [0001] growth direction. (H) Two- and four-probe $I-V$ characteristics for the NW with the [0001] growth direction.

and HRTEM image (Figure 1I) confirm that the growth direction is [0001].

In order to correlate the electrical properties with structure in anisotropic In_2Se_3 NWs with different growth directions, we exploited a technique combining HRTEM and single NW electrical transport measurement (Figure 2A). The individual In_2Se_3 NW devices were fabricated directly on a 50 nm thick SiN_x membrane of TEM grids, which is thin enough to be transparent to the high-energy electron beam in TEM. In_2Se_3 NWs were first mechanically transferred onto the SiN_x membrane with microelectrodes and alignment markers prefabricated by electron beam lithography (EBL), followed by a second step of EBL to define multiple metal contacts. In/Au (50 nm In and 70 nm Au) is used as the contact metal, which we found to form nearly ohmic contact without any annealing.

Figure 2B shows a scanning electron microscopy (SEM) image of a NW TEM grid device over large area. The large metal pads are used to connect with external measurement electronics. Figure 2C shows a TEM image of a NW contacted by seven In/Au electrodes on the SiN_x membrane. The NW has uniform diameter along the NW length. Now let us focus on a 630 nm long segment between the two electrodes (Figure 2C dashed frame, Figure 2D). The HRTEM images (Figure 2E,G) indicate that the growth direction of the NW is [0001], confirmed by the corresponding SAED pattern (Figure 2F). The diameter of the NW is ~125 nm. The electronic transport measurements were carried out at room temperature before TEM imaging to

avoid possible e-beam damage. The source-drain current (I) versus voltage (V_{sd}) characteristic is linear and symmetric, with a two-probe resistance of 50 MΩ (Figure 2H). To extract the intrinsic NW resistance from the contact resistance, we also carried out four-probe measurements. The four-probe resistance is 23.8 MΩ, and the contact resistance is 13.1 MΩ per contact. The intrinsic NW conductivity is calculated to be ~0.02 S/cm. Our measurements on 10 NW TEM devices (channel length < 1 μm) with the [0001] growth direction show an intrinsic conductivity in the range of 0.005−0.025 S/cm.

We also carried out the TEM and single NW electrical transport studies on In_2Se_3 NWs along the [11−20] growth direction. The SEM image (Figure 3A) and the corresponding TEM image (Figure 3B) show a straight NW with 1.05 μm between In/Au contacts on a 50 nm thick SiN_x membrane window. The magnified TEM image (Figure 3C) shows the straight NW has a uniform width of 60 nm. The thickness of the NW is about 25 nm according to the atomic force microscopy (AFM) measurements. HRTEM study (Figure 3D) demonstrates clearly that the NW is single-crystal hexagonal In_2Se_3 with a fourfold superlattice structure across the NW width. The corresponding SAED pattern (Figure 3E) can be indexed to the hexagonal structure of In_2Se_3 with the zone axis along the [0001] direction. The NW growth direction is along [11−20] and the superlattice diffraction spots are also clearly observed. Figure 3F shows that the room-temperature $I-V$ curve is linear with a resistance of 30.3 KΩ. The linear $I-V$ curve and low resistance indicate

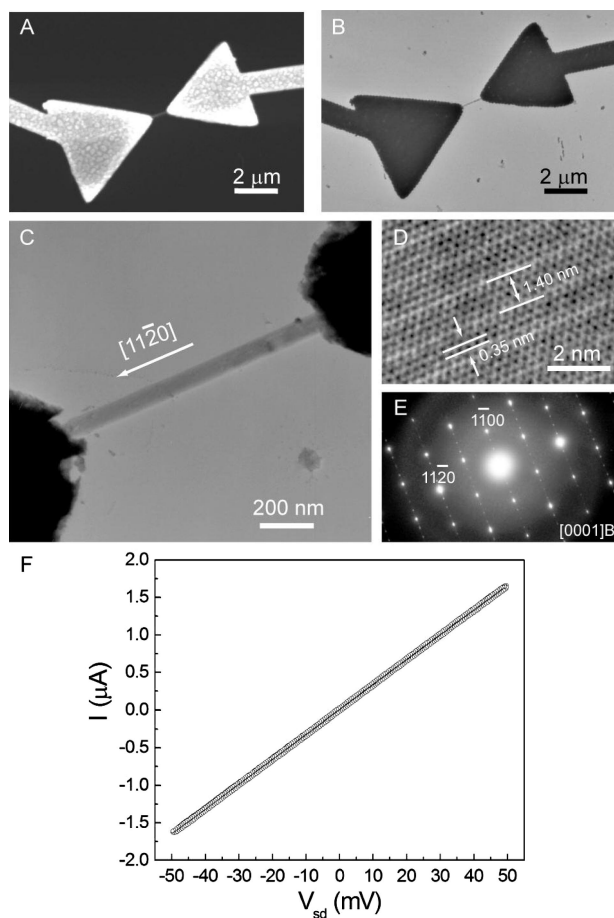**Figure 4.** (A) SEM image of a NW with the [11−20] growth direction contacted with In/Au electrodes on the SiN$_x$/Si subtrate. (B) Two-probe $I-V$ characteristics for the NW with the [11−20] growth direction at 4.6 and 290 K. (C) Temperature-dependent normalized resistances obtained from the same device; the resistance, R, is normalized by the value at 290 K, R_0. (D) Source-drain current versus gate voltages (V_g) curves with $V_{sd} = 10$ mV recorded at 8 and 290 K.

Figure 3. (A) SEM image of a NW with the [11−20] growth direction contacted with In/Au electrodes on TEM grid. (B) Corresponding TEM image of the NW contacted with In/Au electrodes. (C) A magnified TEM image of the NW between the electrodes. (D) HRTEM image of NW with superlattice structure perpendicular to the [11−20] growth direction. (E) Corresponding SAED pattern. (F) Two-probe $I-V$ characteristic for the NW with the [11−20] growth direction.

that the contact is nearly ohmic so that we can use two-terminal resistance to estimate the intrinsic NW conductivity. The conductivity of this NW along the [11−20] direction ($\sigma_{//}$) is ∼230 S/cm, which is ∼10^4 times more conductive than the NW with the [0001] growth direction ($\sigma_\perp$). The large conductivity difference suggests a strong anisotropy in the layered In$_2$Se$_3$.

To study the gate-dependent electrical properties, the In$_2$Se$_3$ NW devices were fabricated on a 170 nm thick SiN$_x$ layer with the underlying conducting Si substrate as a back gate. Now even without TEM structure data, we can differentiate NWs with different growth directions by their significant difference in conductivity. Figure 4A shows a typical [11−20] In$_2$Se$_3$ NW with a channel length of 1.9 μm between In/Au contacts. The width is about 165 nm, and the height is about 30 nm from AFM measurements, which is a nanoribbon shape consistent with the [11−20] In$_2$Se$_3$ NWs. Figure 4B shows linear $I-V$ behavior with a resistance of 11.8 KΩ at 290 K (conductivity ∼ 320 S/cm). Measurements conducted over 50 NW devices show that the conductivity of In$_2$Se$_3$ NW with [11−20] growth direction
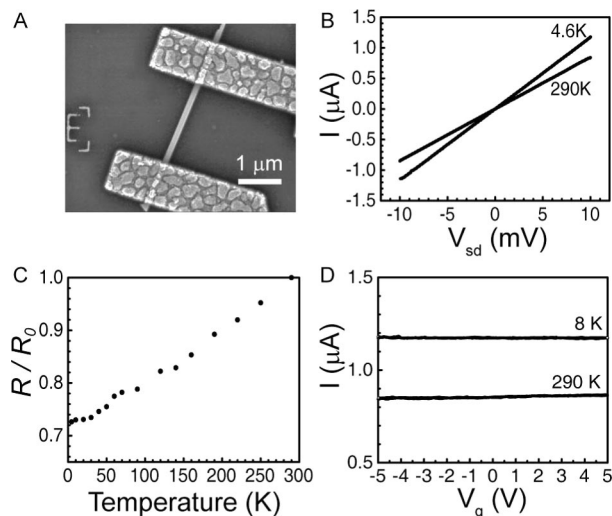
is in the range of 100−500 S/cm. Temperature-dependent electrical transport measurements were carried out to further characterize the [11−20] NWs. The linear $I-V$ is maintained even if the sample is cooled down to 4.6 K (Figure 4B). The NW resistance decreases monotonically with temperature down to 4.6 K, suggesting metallic behavior (Figure 4C). For the temperature range studied (290 to 8 K), the [11−20] NWs do not exhibit gate-dependence, confirming metallic behavior (Figure 4D). These data are surprising since In$_2$Se$_3$ is usually known as a semiconductor with a band gap of about 1.3 eV.[32,33] Our observed metallic behavior in NWs is likely due to the superlattice ordering. It was suggested that a small fraction of In atoms (∼6.25%) can be shifted to the six-coordinated interstices of Se atoms from the four-coordinated interstices only by small movement, which changes the electronic band structure from semiconductor to metal.[32] The metallic In$_2$Se$_3$ has indeed been observed in quench-prepared bulk In$_2$Se$_3$.[17,34,35]

In contrast to the metallic behavior of In$_2$Se$_3$ NW grown along the [11−20] direction, the NW with the [0001] growth direction shows semiconductive behavior. Figure 5A shows a NW device consisting of an 80 nm diameter In$_2$Se$_3$ NW along the [0001] growth direction on the SiN$_x$/Si substrate. The channel length of NW is about 1.6 μm. Figure 5B shows $I-V$ behavior with a two-terminal resistance of 5.9 GΩ at room temperature. The calculated two-terminal conductivity of the NW device here is about 5.4 × 10^{-4} S/cm, and the intrinsic conductivity is estimated to be in the same order of magnitude. Gate voltage-dependent transport measurements were also carried out at room temperature. Figure 5C shows $I-V$ curves at different gate voltages (V_g). Figure 5D shows the $I-V_g$ curve at fixed $V_{sd} = 50$ mV. When V_g is made increasingly negative (positive), the conductance decreases (increases). This gate dependence shows that the [0001]
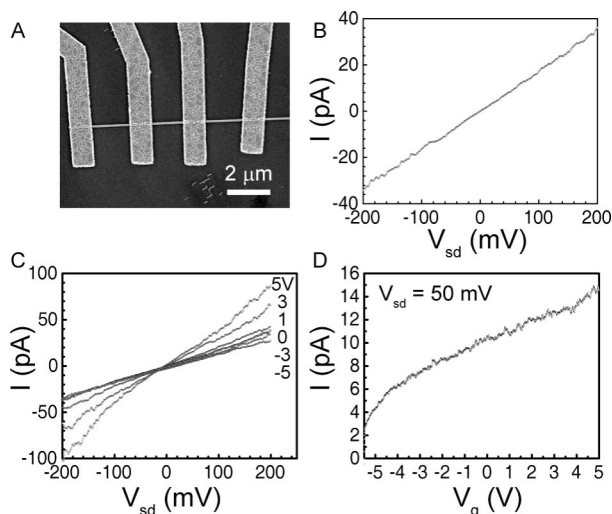
Figure 5. (A) SEM image of a NW with the [0001] growth direction contacted with In/Au electrodes on the SiN$_x$/Si substrate. (B) Two-probe $I-V$ characteristic recorded on a 1.6 μm channel length NW with the [0001] growth direction at room temperature. (C) $I-V_{sd}$ curves obtained from the same device at different gate voltages. (D) Gate sweep obtained from the same device with V_{sd} = 50 mV.

In$_2$Se$_3$ NW is an n-type semiconductor, consistent with bulk In$_2$Se$_3$.[34,36] NWs with the [0001] growth direction have an additional difference from NWs with the [11−20] growth direction. The weak interaction between the layers along the [0001] direction can cause structure defects such as stacking faults more easily. The frequency of stacking faults is increased with the NW lengths. Our electrical measurements on the long channel devices (typically >1.5 μm) of NWs with the [0001] direction show conductivity values 1−2 orders of magnitude lower than the short channel ones (<1 μm; see Supporting Information). Such a strong channel-length dependence of conductivity is not observed for the NWs with the [11−20] growth direction (see Supporting Information). The anisotropic ratio of conductivity for the long channel devices can be up to 10^6, which is significantly higher than the bulk ratio (up to ~10^3).[35,36] It is most likely because a NW has a pure α-phase structure and is a single domain while bulk In$_2$Se$_3$ single crystal often has mixed phases and multiple phase domains.[27,36] Therefore, NWs provide much more well-defined samples than bulk materials for studying the intrinsic anisotropic properties.

In summary, we have developed a powerful technique combining HRTEM investigation and single NW electrical transport measurement, which allows us to correlate directly the electrical properties and structure of the same individual In$_2$Se$_3$ NWs with a large anisotropy in shape and crystal structure. The electrical conductivity, gate response, and temperature dependence are distinct for NWs with different growth directions. Layered NWs with a one-dimensional superlattice structure perpendicular to the [11−20] growth direction exhibit metallic behavior while the NWs grown along the [0001] direction show n-type semiconductive behavior. The conductance anisotropy is in the range of 10^3−10^6 at room temperature, which is 1−3 orders of magnitude higher than the bulk ratio.[35,36] This technique

combining HRTEM study and single NW electrical transport measurement could open up opportunities for fundamental and applied studies of nanoelectronics, solar cells, and phase-change memories.

Supporting Information Available: Length dependence of the measured conductivities for In$_2$Se$_3$ nanowires with the two growth directions. This material is available free of charge via the Internet at http://pubs.acs.org.

References

(1) Bjork, M. T.; Ohlsson, B. J.; Thelander, C.; Persson, A. I.; Deppert, K.; Wallenberg, L. R.; Samuelson, L. *Appl. Phys. Lett.* **2002**, *81*, 4458–4460.
(2) Cui, Y.; Lieber, C. M. *Science* **2001**, *291*, 851–853.
(3) Gudiksen, M. S.; Lauhon, L. J.; Wang, J.; Smith, D. C.; Lieber, C. M. *Nature* **2002**, *415*, 617–620.
(4) Huang, M. H.; Mao, S.; Feick, H.; Yan, H. Q.; Wu, Y. Y.; Kind, H.; Weber, E.; Russo, R.; Yang, P. D. *Science* **2001**, *292*, 1897–1899.
(5) Cui, Y.; Wei, Q. Q.; Park, H. K.; Lieber, C. M. *Science* **2001**, *293*, 1289–1292.
(6) Hochbaum, A. I.; Chen, R.; Delgado, R. D.; Liang, W.; Garnett, E. C.; Najarian, M.; Majumdar, A.; Yang, P. *Nature* **2008**, *451*, 163–167.
(7) Boukai, A. I.; Bunimovich, Y.; Tahir-Kheli, J.; Yu, J.-K.; Goddard, W. A.; Heath, J. R. *Nature* **2008**, *451*, 168–171.
(8) Tian, B.; Zheng, X.; Kempa, T. J.; Fang, Y.; Yu, N.; Yu, G.; Huang, J.; Lieber, C. M. *Nature* **2007**, *449*, 885–889.
(9) Chan, C. K.; Peng, H.; Liu, G.; McIlwrath, K.; Zhang, X. F.; Huggins, R. A.; Cui, Y. *Nature Nanotechnology* **2008**, *3*, 31–35.
(10) Law, M.; Greene, L. E.; Johnson, J. C.; Saykally, R.; Yang, P. D. *Nat. Mater.* **2005**, *4*, 455–459.
(11) Wang, Z. L.; Song, J. H. *Science* **2006**, *312*, 242–246.
(12) Wang, X. D.; Song, J. H.; Liu, J.; Wang, Z. L. *Science* **2007**, *316*, 102–105.
(13) Kuykendall, T.; Pauzauskie, P. J.; Zhang, Y.; Goldberger, J.; Sirbuly, D.; Denlinger, J.; Yang, P. *Nat. Mater.* **2004**, *3*, 524–528.
(14) Lieber, C. M. *MRS Bull.* **2003**, *28*, 486–491.
(15) Yang, P. D. *MRS Bull.* **2005**, *30*, 85–91.
(16) Kwon, S. H.; Ahn, B. T.; Kim, S. K.; Yoon, K. H.; Song, J. *Thin Solid Films* **1998**, *323*, 265–269.
(17) Julien, C.; Hatzikraniotis, E.; Chevy, A.; Kambas, K. *Mater. Res. Bull.* **1985**, *20*, 287–292.
(18) Lee, H.; Kang, D. H.; Tran, L. *Mater. Sci. Eng. B: Solid State Mater. Adv. Technol.* **2005**, *119*, 196–201.
(19) Lee, H.; Kim, Y. K.; Kim, D.; Kang, D. H. *IEEE Transactions on Magnetics* **2005**, *41*, 1034–1036.
(20) Lankhorst, M. H.; Ketelaars, B. W.; Wolters, R. A. *Nat. Mater.* **2005**, *4*, 347–352.
(21) Peng, H. L.; Schoen, D. T.; Meister, S.; Zhang, X. F.; Cui, Y. *J. Am. Chem. Soc.* **2007**, *129*, 34–35.
(22) Sun, X. H.; Yu, B.; Ng, G.; Nguyen, T. D.; Meyyappan, M. *Appl. Phys. Lett.* **2006**, *89*, 23–25.
(23) Ye, J. P.; Soeda, S.; Nakamura, Y.; Nittono, O. *Jpn. J. Appl. Phys.* **1998**, *37*, 4264–4271.
(24) Pan, Z. W.; Dai, Z. R.; Wang, Z. L. *Science* **2001**, *291*, 1947–1949.
(25) Peng, H. L.; Meister, S.; Chan, C. K.; Zhang, X. F.; Cui, Y. *Nano Lett.* **2007**, *7*, 199–203.
(26) Peng, H.; Xie, C.; Schoen, D. T.; McIlwrath, K.; Zhang, X. F.; Cui, Y. *Nano Lett.* **2007**, *7*, 3734–3738.
(27) Vanlanduyt, J.; Vantendeloo, G.; Amelinckx, S. *Phys. Status Solidi A: Appl. Res.* **1975**, *30*, 299–314.
(28) Semiletov, S. A. *Sov. Phys. Crystallogr.* **1961**, *6*, 158–160.
(29) Han, W.-Q.; Wu, L.; Stein, A.; Zhu, Y.; Misewich, J.; Warren, J. *Angew. Chem.* **2006**, *118*, 6704–6708.
(30) Ding, Y.; Morber, J. R.; Snyder, R. L.; Wang, Z. L. *Adv. Funct. Mater.* **2007**, *17*, 1172–1178.
(31) Lee, Y. C.; Chueh, Y. L.; Hsieh, C. H.; Chang, M. T.; Chou, L. J.; Wang, Z. L.; Lan, Y. W.; Chen, C. D.; Kurata, H.; Isoda, S. *Small* **2007**, *3*, 1356–1361.

(32) Watanabe, Y.; Kaneko, S.; Kawazoe, H.; Yamane, M. *Phys. Rev. B* **1989**, *40*, 3133–3142.

(33) Julien, C.; Chevy, A.; Siapkas, D. *Phys. Status Solidi A* **1990**, *118*, 553–559.

(34) Julien, C.; Hatzikraniotis, E.; Kambas, K. *Phys. Status Solidi A* **1986**, *97*, 579–585.

(35) Bidjin, D.; Popovic, S.; Celustka, B. *Phys. Status Solidi A* **1971**, *6*, 295–299.

(36) Fotsing, J.; Julien, C.; Balkanski, M. *Mater. Sci. Eng.* **1988**, *B1*, 139–145.